Electron heating mechanisms in dual frequency capacitive discharges

M M Turner[1] and P Chabert[2]

[1]School of Physical Sciences and National Centre for Plasma Science and Technology, Dublin City University, Dublin 9, Ireland

[2]Laboratoire de Physique et Technologie des Plasmas, Ecole Polytechnique, 91128 Palaiseau, France

E-mail: `miles.turner@dcu.ie`

Abstract. We discuss electron heating mechanisms in the sheath regions of dual-frequency capacitive discharges, with the twin aims of identifying the dominant mechanisms and supplying closed-form expressions from which the heating power can be estimated. We show that the heating effect produced by either Ohmic or collisionless heating is much larger when the discharge is excited by a superposition of currents at two frequencies than if either current had acted alone. This coupling effect occurs because the lower frequency current, while not directly heating the electrons to any great extent, strongly affects the spatial structure of the discharge in the sheath regions.

PACS numbers:

Submitted to: *Plasma Sources Sci. Technol.*

1. Introduction

Great interest is presently directed towards capacitive discharges excited by a superposition of currents at two or more frequencies. This interest is motivated by a desire to control the plasma parameters with more freedom than is possible when only a single frequency is employed. In a typical dual-frequency discharge, the two frequencies are disparate, with a ratio of at least ten. Moreover, the current density at the higher frequency is larger than that at the lower frequency. As the impedance is predominantly capacitive, and therefore decreasing with frequency, one typically finds that the voltage associated with the lower frequency is larger than the voltage associated with the higher frequency. The advantage of this configuration is that the plasma density, and hence the ion flux at the plasma boundary, depends primarily on the current density, and this is controlled by the higher frequency, while the ion energy at the boundary depends mainly on the voltage, and this is controlled by the lower frequency. Hence one can hope to exert separate control over the ion flux and energy by appropriately manipulating the higher and lower frequency current densities. Since the ion flux and energy are crucial parameters in many applications, this is an important advantage. Of course, in practice one does not achieve independent control of these two parameters. Various physical mechanisms produce coupling between the two frequencies, and these effects have been explored in general terms in a number of recent papers, *e.g.* [1, 2, 3, 4, 5, 6]. The purpose of the present paper is to discuss the electron heating mechanisms that operate in dual-frequency discharges—in particular, to elucidate their nature and significance, and as far as possible supply convenient formulae that may be used as elements in a comprehensive theoretical understanding of these discharges. Recent work on collisionless heating by capacitive sheaths has pursued different theoretical paths and adopted different procedures for comparing theory and simulations [7, 8, 9, 10, 11]. However, the upshot is similar scaling laws and absolute differences of approximately a factor of two. Our present purpose is not to investigate the reasons for these relatively minor divergences, which are of interest mainly to specialists, but to discuss scaling laws and the relative importance of collisionless and Ohmic heating in dual frequency discharges. The present paper, therefore, elaborates on the argument of [9] and supplies a somewhat different view of the problem than that of [10].

For the purpose of our discussion, we assume that the discharge is divisible into two kinds of region: namely, bulk plasma—where quasi-neutrality always holds and the plasma density is time-independent—and sheaths,where the electron density at least may be strongly varying in time, and where consequently gross departures from quasi-neutrality may occur. We further assume that electron heating in bulk regions is predominantly Ohmic in character, and as the problem of calculating the amount of Ohmic heating in a region of stationary plasma parameters is a simple one [12], we will not devote space to that topic. The focus of this paper is, therefore, to investigate the electron heating that occurs in sheath regions, where the electron density varies strongly in time. Electron heating in this case is some mixture of Ohmic heating and collisionless

(also called stochastic) heating. We will show that for both of these mechanisms, the magnitude of the heating effect is strongly influenced not only by the higher frequency current density, but also by the lower frequency current density. However, the means by which this influence is exerted is different for the two frequencies. The higher frequency acts in the usual way, by producing an oscillatory motion of the electrons that is damped in some way to produce heating, but the lower frequency affects the heating indirectly by changing the structure of the sheath. In the presence of the lower frequency, the sheath is wider, and the gradient of plasma density is steeper. As we will show, this greatly enhances both Ohmic and collisionless heating.

In the discussion that follows, we assume that the spatial and temporal structure of the sheath region is adequately described by the analytical model of [13, 14]. That model has limitations, most notably that it requires the higher frequency voltage to be small compared to the lower frequency voltage, and this prevents us from directly calculating the heating effects in certain interesting cases, as we show below. However, this model has the important advantage that it is strictly analytical, and supplies tractable formulae for the discharge parameters of primary concern, which is not altogether true of the other models that we might have chosen [15, 16]. We adopt from these models a simplified representation of the spatial structure of the sheath, in which the transition between the quasi-neutral plasma and the space-charge sheath is modelled as a step-function in the electron density. Since the ion density is assumed to be time independent, the sheath dynamics are captured by specifying the position of this electron density step as a function of time. In the discussions that follow, we denote the position of this electron sheath edge by $x = s(t)$, and we adopt the convention that the ion sheath edge, where the ions reach the Bohm velocity, is at $x = 0$, so that the electrode is at $x = s_{\max}$. In a dual-frequency discharge, the trajectory of the electron sheath edge is complex, but bounded in the range $0 \leq s(t) \leq s_{\max}$. We assume that the current passing through the sheath is the superposition of two frequencies, so that

$$J(t) = -\tilde{J}_l \sin \omega_l t - \tilde{J}_h \sin \omega_h t, \tag{1}$$

where $\tilde{J}_{l,h}$ and $\omega_{l,h}$ are the current densities and angular frequencies of the two components. (The surprising sign convention is chosen for consistency with previous works [17, 13].) Robiche *et al* [13] have shown that under these assumptions, the sheath dynamics are adequately described by three dimensionless parameters, the ratio of current frequencies, $\alpha \equiv \omega_h/\omega_l$, the ratio of current densities, $\beta \equiv \tilde{J}_h/\tilde{J}_l$, and $H_l \equiv \tilde{J}_l^2/\pi T \omega_l^2 n_0$, subject to approximations that hold when $\beta/\alpha \ll 1$. The parameter H was introduced in the single frequency sheath model of Lieberman [17]. An important point is that the equivalent of the Lieberman H parameter for this dual-frequency sheath model does not depend on higher frequency parameters, ω_h and $\tilde{J}_h$, which shows that the lower-frequency essentially controls the spatial structure of the sheath. As we will see, this is a crucial point with profound implications for the interaction of the frequencies in a dual-frequency discharge.

In what follows, we first discuss separately the two heating mechanisms that we

consider, and we develop detailed theories of each. We show that these theories can be reduced to convenient closed expressions that should be useful for analytical model development, and in other contexts, such as analysis of experiments. In a final section, we discuss the relative importance of collisionless and Ohmic heating. We show that, while both mechanisms are strongly influenced by nonlinear interaction between the lower and higher frequencies, the affect on Ohmic heating is more marked, with the result that a heating mode transition can be induced by manipulating the current densities. In particular, a transition from a state where collisionless heating is dominant to one where Ohmic heating is dominant can take place when the current density as the lower frequency is increased.

2. Collisionless heating

We consider a plasma consisting of electrons and one species of positive ion. Both electrons and ions are assumed collisionless. An electrode is in contact with the plasma, and this electrode carries a net current density given by eq. 1. We assume that the collisionless heating effect occurs in the electron fluid, in the region between the electron and ion sheath edges, as in [7]. This region is described by the Vlasov-Poisson system of equations, with one real space dimension and one velocity space dimension. Using moments of the Vlasov equation, we can show that the electron fluid is described by:

$$\frac{\partial}{\partial t}\left(\frac{1}{2}nT\right)+\frac{\partial}{\partial x}\left(\frac{3}{2}nuT+Q\right)-u\frac{\partial}{\partial x}\left(nT\right)=0. \tag{2}$$

where n is the density, T is the temperature expressed in joules, u is the drift velocity and Q is the heat flux. We note that T characterizes the non-drifting part of the electron velocity distribution, and it is not implied or entailed that this is Maxwellian. If the non-drifting portion of the electron velocity distribution function were Maxwellian, the heat flux would vanish, and this would be inconsistent with our theory. So it is actually *required* that the non-drifting portion of the electron velocity distribution function is not Maxwellian.

In accordance with the discussion above, we assume that the positive ion density n_i is given by a suitable sheath model [13, 16], and that in this quasi-neutral region $n \simeq n_i$, so n is given. From the specification of the current density, eq. 1, it follows that

$$\int_0^{s(t)} n\ dx = n_0\left\{\frac{\tilde{u}_l}{\omega_l}\left(1-\cos\omega_l t\right)+\frac{\tilde{u}_h}{\omega_h}\left(1-\cos\omega_h t\right)\right\} \tag{3}$$

$$-u_0 n_0 \quad = n_0\left(\tilde{u}_l\sin\omega_l t+\tilde{u}_h\sin\omega_h t\right), \tag{4}$$

where $\tilde{u}_l=\tilde{J}_l/en_0$, *etc*, and the subscript 0 refers to quantities defined at the ion sheath edge. We assume that T is independent of x within the sheath. This is reasonable *a priori*, because the wavelength of thermal disturbances in the electron fluid is large compared to the sheath length, and is also reasonable with reference to the kinetic simulation results discussed below. If T can be assumed spatially constant, we can integrate eq. 2 between the ion sheath edge and the electron sheath edge to obtain the

ordinary differential equation

$$\frac{1}{2}n_0\frac{dT}{dt}\left\{\frac{\tilde{u}_l}{\omega_l}\left(1-\cos\omega_l t\right)+\frac{\tilde{u}_h}{\omega_h}\left(1-\cos\omega_h t\right)\right\}$$
$$-Tn_0\ln\left(\frac{n_s}{n_0}\right)\left(\tilde{u}_l\sin\omega_l t+\tilde{u}_h\sin\omega_h t\right) \qquad -2Q_b\left(\frac{T}{T_b}\right)\left(1-\frac{T}{T_b}\right)=0, \tag{5}$$

where $Q_b=\frac{1}{4}n_0\bar{v}_bT_b$, $\bar{v}_b=\sqrt{8T/\pi m_e}$, the subscript s denotes quantities defined at the electron sheath edge and T_b is the temperature of the electron flux incident from the bulk plasma. This equation assumes that no electrons are absorbed by the electrode. Eq. 5 apparently contains six autonomous physical parameters, namely T_b, n_0, $\tilde{J}_l$, ω_l, $\tilde{J}_h$ and ω_h. These, however, can be reduced to the four dimensionless parameters, $\delta_l\equiv\tilde{u}_l/\bar{v}_b$, $\gamma_l\equiv\omega_l/\omega_p$, $\delta_h\equiv\tilde{u}_h/\bar{v}_b$ and $\gamma_h\equiv\omega_h/\omega_p$, where $\omega_p^2\equiv e^2n_0/\epsilon_0m_e$. We define $n_s(t)$ using the sheath model of [13], which has the three control parameters discussed above, which can be written as $\alpha=\gamma_h/\gamma_l$, $\beta=\delta_h/\delta_l$ and $H_l\equiv 8\delta_l^2/\pi^2\gamma_l^2$. With the normalizations $\tau\equiv T/T_b$ and $\theta\equiv\omega_l t$, eq. 5 can be written:

$$\delta_l\left[\left(1-\cos\theta\right)\frac{d\tau}{d\theta}-2\tau\ln\eta\sin\theta\right]$$
$$+\delta_h\left[\frac{1}{\alpha}\left(1-\cos\alpha\theta\right)\frac{d\tau}{d\theta}-2\tau\ln\eta\sin\alpha\theta\right]+\tau\left(\tau-1\right)=0, \tag{6}$$

where $\eta\equiv n_s/n_0$.

Eq. 6 is solved by an expression in the form:

$$\tau=\tau^{(0)}+\delta_l\tau_l^{(1)}+\delta_h\tau_h^{(1)}+\delta_l^2\tau_l^{(2)}+\delta_h^2\tau_h^{(2)}+\delta_l\delta_h\tau_{hl}^{(2)}+\mathrm{O}(\delta_{l,h}^3), \tag{7}$$

where the $\tau^{(n)}$ are arbitrary functions that are to be determined by inserting the power series, eq. 7, into the differential equation, eq. 6. Since $\delta_{l,h}\ll 1$, the series may be truncated if α is not too large, and in this way, we find

$$\tau^{(0)}=1 \tag{8}$$
$$\tau_l^{(1)}=2\ln\eta\sin\theta \tag{9}$$
$$\tau_h^{(1)}=2\ln\eta\sin\alpha\theta \tag{10}$$
$$\tau_l^{(2)}=-\left(1-\cos\theta\right)\frac{d\tau_l^{(1)}}{d\theta} \tag{11}$$
$$\tau_h^{(2)}=-\frac{1}{\alpha}\left(1-\cos\alpha\theta\right)\frac{d\tau_h^{(1)}}{d\theta} \tag{12}$$
$$\tau_{lh}^{(2)}=-\left(1-\cos\theta\right)\frac{d\tau_h^{(1)}}{d\theta}-\frac{1}{\alpha}\left(1-\cos\alpha\theta\right)\frac{d\tau_l^{(1)}}{d\theta}. \tag{13}$$

We can now express the sheath heating power per unit area as:

$$\langle S_{lh}\rangle=-\langle Q_0\rangle=2Q_b\tau(\tau-1) \tag{14}$$
$$=2Q_b\left\langle\delta_l^2\left(\tau_l^{(2)}+{\tau_l^{(1)}}^2\right)+\delta_h^2\left(\tau_h^{(2)}+{\tau_h^{(1)}}^2\right)\right\rangle, \tag{15}$$

as $\langle\tau_l^{(1)}\rangle=\langle\tau_h^{(1)}\rangle=\langle\tau_{lh}^{(2)}\rangle=0$. We note that the instantaneous heating power in eq. 14 is not identical with the integral of the product JE from $x=0$ to $x=s(t)$, because

both the drift energy and the thermal energy of the electron fluid in this region vary with time. However, the time average of this spatial integral of JE and the time average given by eq. 14 are identical. Two integrals remain to be evaluated:

$$F_0(H_l, \alpha, \beta) = \frac{1}{2\pi} \int_0^{2\pi} \left(\tau_l^{(2)} + {\tau_l^{(1)}}^2 \right) d\theta \tag{16}$$

$$F_1(H_l, \alpha, \beta) = \frac{1}{2\pi} \int_0^{2\pi} \left(\tau_h^{(2)} + {\tau_h^{(1)}}^2 \right) d\theta. \tag{17}$$

These expressions cannot be evaluated analytically, not least because of the complex expressions that are introduced from the sheath model into the definitions of $\tau_l^{(1)}$, *etc.* However, we can find convenient approximate results that will hold in most cases of practical interest. We note first that the integrand in I_0 depends on the parameters H_l, α and β only through the sheath model, that is to say through the definition of $\ln \eta \equiv n_s(H, \alpha, \beta)/n_0$. The parameters α and β introduce local oscillatory behaviour that is not important to the period average, such that it is a good approximation to set $\beta = 0$ in the integrand of I_0. (This is equivalent to approximating the dual frequency sheath model of [13] with the single frequency model of [17].) With this simplification, I_0 is a function of H_l only, and is identical to the integral discussed in [7], which is there asserted to be well approximated by:

$$F_0(H_l, \alpha, \beta) \approx A_0(H_l) = \frac{36 H_l}{55 + H_l}. \tag{18}$$

We can approach F_1 in a similar manner. In this case, the integrand depends explicitly on α because the functions $\tau_h^{(1)}$ and $\tau_h^{(2)}$ depend on α, so this integral cannot be reduced in exactly the same way as I_0. However, I_1 is similarly insensitive to the values of α and β, and by reference to numerical evaluation of F_1 using a quadrature method we find that:

$$F_1(H_l, \alpha, \beta) \approx A_1(H_l) = 1.1 \frac{36 H_l}{55 + H_l}. \tag{19}$$

In fig. 1, we compare the value of F_1 computed by a quadrature with the approximation indicated in eq. 19. This shows that the approximation is good for a wide range of values of α, in particular. With these expressions for the values of the integrals, we can write a compact expression for the net heating when both frequencies act together:

$$\langle S_{lh} \rangle \approx 2 Q_b \left(\delta_l^2 + 1.1 \delta_h^2 \right) A_1(H_l). \tag{20}$$

We will now discuss the predictions of this model with reference to particle-in-cell simulations [18]. Our procedure is described in detail in [19], therefore we give only brief particulars. We simulate only the sheath and its immediate vicinity, by injecting electrons and ions from one boundary with velocity distributions chosen to model an adjacent semi-infinite plasma with a given electron temperature and density. Electrons are injected with distribution corresponding to a Maxwellian bulk plasma, while ions are initially injected with a drift velocity at the Bohm speed and a thermal component at 350 K. We allow this simulation to proceed in time until a harmonic steady state is reached with respect to both driving frequencies. Then, we freeze the ions, so that

electrons ceases to be collected by the electrode. In this way, we reproduce in the simulation the situation envisaged in the model discussed above, and we separate the collisionless heating effect from extraneous phenomena that would otherwise complicate our interpretation of the simulation results. The physical parameters used in these calculations are $n_0 = 5 \times 10^{15}$ m^{-3} and $T_b = 30000$ K. Except where otherwise implied, $\omega_l = 2\pi \times 2$ MHz, $\omega_h = 2\pi \times 26$ MHz, $\tilde{J}_l = 10$ A m^{-2} and $\tilde{J}_h = 36$ A m^{-2}

Indications of the general character of the heating effect, and the consistency of the simulations with the model, are shown in figs. 2 and 3. Fig 2 is an example of the heating power per unit area computed from the simulation. This figure shows that the heating power reaches a positive maximum during the expanding phase of the low-frequency sheath, where $\pi < \theta < 2\pi$, a feature which is also seen in the analytical model. In fig. 3, we compare the sheath electron temperature from the simulation with the analytical model, and we find generally good agreement. More detailed parametric investigations are shown in figs. 4 and 5. Fig. 4 shows excellent agreement between the simulations and the model for a moderate value of α. However, fig. 5 shows that this is not sustained for much larger α. There are two reasons for this. One is that there is a dependency on α that the analytic solution fails to capture when α is large, and this is a failure of the power series solution, not the approximations made between eqs. 15 and 20. The solution procedure is not as mathematically robust when applied to this dual-frequency model as was the case in [7]. In that work, a necessary and sufficient condition for the power series approximation to converge was that $\delta \ll 1$, and this is satisfied for any reasonable choice of the physical parameters. In the present case, we must also have $\delta_l \alpha \ll 1$, and this condition is not automatically satisfied for all reasonable choices of the physical parameters. This is a limitation of the method of the solution, however, not of the physical model. Although the analytical solution does not capture the frequency scaling effects, these are correctly recovered when eq. 6 is solved numerically, as fig. 5 shows. In addition, at the extreme upper range of α that we considered, ω_h/ω_p is not very small, and one begins to see strong excitation of electron plasma waves at the plasma sheath boundary, and perhaps also excitation of other related resonances. These effects are not included in our model. It is not clear whether they directly effect electron heating, or exert influence via a modification of the sheath structure.

Our model entails surprising predictions: Namely, that the heating power does not depend on the parameter H_h and cannot be expressed as if the two frequencies acted additively. As we suggested above, the spatial structure of the sheath is controlled by low-frequency parameters, with the result that the heating power is enhanced when the two frequencies act together, because $F_2(H_l) \gg F_2(H_h)$ and $\delta_h^2 \gg \delta_l^2$, where we recall that $\delta_{l,h} \propto \tilde{J}_{l,h}$. Specifically, since

$$\frac{\langle S_{lh} \rangle}{\langle S_l \rangle + \langle S_h \rangle} \approx \frac{1 + 1.1\beta^2}{1 + \beta^4/\alpha^2} \tag{21}$$

when $H_{l,h}$ are not too large so $A_2(H) \sim 36H/55$, the maximum enhancement is approximately $(1+\alpha)/2$, which occurs when $\beta \approx \sqrt{\alpha}$. These parameters are within the

typical range of current experiments. The enhancement occurs because the application of the low frequency changes the sheath structure, allowing the high frequency to explore a much wider dynamic range of plasma density. In fig. 6, we compare the heating effect produced by each frequency separately with their combined effect, showing that the predicted enhancement does exist. In the case shown, which is close to the predicted maximum with $\beta/\sqrt{\alpha} \sim 1$, the enhancement factor is approximately 5, compared to the predicted 7. The discrepancy is mostly because H_h is significantly less than 1, and the single frequency theory is not highly accurate in that case. We note that the application of the low frequency produces an appreciable expansion of the volume of plasma affected by the heating process.

We note that in the present theory, the average heating power is exactly zero on the plasma side of the ion sheath edge, because both n and T are assumed to be uniform in that region. In simulation, and presumably in experiments, there is a region of negative heating in the bulk plasma adjacent to the sheath, which is clearly visible in fig. 6. This effect has been discussed elsewhere for the single frequency case [20, 21, 8]. The origin is essentially a thermal disturbance, *i.e.* T is not spatially uniform,

The theory we have been discussing cannot presently be extended by formal means to the interesting limit $J_l \to 0$, because the sheath model of [13] is not valid in that case. However, a simple ansätz allows us to construct an extension that connects the present dual frequency theory smoothly to the single frequency theory of [7]. This ansätz entails the definition of an effective value of the parameter H that is given by

$$H_{\text{eff}} = \sqrt{H_l^2 + H_h^2}. \tag{22}$$

If this effective value is inserted into eq. 20, an expression is obtained that is essentially identical with the present theory when $H_l \gg H_h$, almost identical with the results of [7] when $H_l \ll H_h$, and reasonably behaved in the transition between these two regimes. In fig. 7, we compare this generalized expression with simulation results.

3. Ohmic heating

In this section, we calculate the Ohmic heating in sheath region of a dual frequency discharge, in which as before we assume that the sheath structure is adequately described by the analytical model of ref. [13]. This is appropriate when then the plasma is weakly collisional, so that the ion transport remains inertia limited. This is probably closer to the typical experimental situation than the friction limited case considered in [15]. Moreover, the model of [15] shares with [22] an inconvenient inconsistency, which prevents the collisionless heating model discussed above from being used with these models. This thwarts one purpose of the present paper, namely the comparison of the significance of Ohmic and collisionless heating that we discuss below. In general, the Ohmic heating power per unit volume dissipated in a plasma with density n and electron collision frequency ν_e is

$$P_{\text{Ohmic}} = \frac{m_e \nu_e J^2}{n e^2} \tag{23}$$

where J is the current density, and we have assumed that any ionic contribution to the heating effect is negligible. The Ohmic power dissipation per unit area within the sheath is now found by integrating from the ion sheath edge located at $x = 0$ to the instantaneous electron sheath edge at $x = s(\phi)$, where $\theta = \omega_l t$:

$$S_{ohmic}(t) = \int_0^{s(\theta)} ds \frac{m_e \nu_e}{n(s) e^2} \left(J_l \sin \omega_l t + J_h \sin \omega_h t\right)^2 \tag{24}$$

$$= \left(J_l \sin \omega_l t + J_h \sin \omega_h t\right)^2 \frac{m_e \nu_e}{e^2} \int_0^{s(\theta)} \frac{ds}{n(s)} \tag{25}$$

$$= \left(J_l \sin \omega_l t + J_h \sin \omega_h t\right)^2 \frac{m_e \nu_e}{e^2} \int_0^{\phi} \frac{d\theta}{n(s)} \frac{ds}{d\theta} \tag{26}$$

These expressions hold for any sheath model. If we assume that the sheath structure is adequately described by the analytical model of [13], then:

$$\frac{ds}{d\theta} = s_0 \left(\sin\theta + \beta \sin \alpha\theta\right) \left(1 + H_l \int_0^{\theta} d\theta' \left(\sin\theta' - \theta' \cos\theta'\right) \left(\sin\theta' + \beta \sin \alpha\theta'\right)\right) \tag{27}$$

and

$$n_i = n_0 \left(1 + H_l \int_0^{\theta} d\theta' \left(\sin\theta' - \theta' \cos\theta'\right) \left(\sin\theta' + \beta \sin \alpha\theta'\right)\right)^{-1} \tag{28}$$

so

$$\int_0^{\theta} \frac{ds}{d\theta'} \frac{d\theta'}{n_i} = \frac{s_0}{n_0} \int_0^{\theta} d\theta' \left(\sin\theta' + \beta \sin \alpha\theta'\right) \times \left(1 + H_l \int_0^{\theta'} d\theta'' \left(\sin\theta'' - \theta'' \cos\theta''\right) \left(\sin\theta'' + \beta \sin \alpha\theta''\right)\right)^2 \tag{29}$$

$$\equiv \frac{s_0}{n_0} F_3(\theta, \alpha, \beta, H). \tag{30}$$

Then:

$$\bar{S}_{\text{ohmic}} = \frac{1}{\pi} \int_0^{\pi} S_{\text{ohmic}} d\theta \tag{31}$$

$$= \frac{2 m_e \nu_e s_0 J_l^2}{e^2 n_0 \pi} \int_0^{\pi} d\theta \left(\sin\theta + \beta \sin \alpha\theta\right)^2 F_3(\theta, \alpha, \beta, H_l) \tag{32}$$

$$= \frac{32}{\pi^2} Q_b \delta_l^3 \left(\frac{\nu_e}{\omega_l}\right) \int_0^{\pi} d\theta \left(\sin\theta + \beta \sin \alpha\theta\right)^2 F_3(\theta, \alpha, \beta, H_l) \tag{33}$$

$$= \frac{32}{\pi} Q_b \delta_l^3 \left(\frac{\nu_e}{\omega_l}\right) F_4(\alpha, \beta, H). \tag{34}$$

We have not sought an exact analytical treatment of the integral F_4, because of the difficulties referred to in [13], *i.e.*, even if an exact result formally exists, it is likely to be unhelpful. However, a convenient approximation can be found that is accurate when $\alpha \gg 1$, which is the limit of primary practical interest. In this case, we can write the integrand in F_4 as a power series in trigonometric functions with argument is $\alpha\theta$. These functions are of course periodic, and vary much more rapidly with θ than the remainder of the integrand. Therefore, we can carry out a local average over

the integrand to remove the explicit dependence on α. With this approximation, the remaining integration can be carried out exactly to find:

$$F_4 \approx A_4 = \left[\frac{1}{2}\left(1+\beta^2\right) + \frac{1}{\pi}\left(\frac{512}{675}+\frac{32}{27}\beta^2\right)H_l + \left(\frac{14912}{165375}+\frac{1336}{3375}\beta^2\right)H_l^2\right]. \quad (35)$$

Fig. 8 compares this approximation with a numerical quadrature of the exact integral, F_4. The approximation is good when $\beta/\alpha \ll 1$, that is, whenever the sheath model of [13] is good, rather independently of the value of H_l. It may be useful to replace H_l in eq. 35 with H_{eff}. This does not yield an entirely satisfactory result, because the limits $\tilde{J}_l \to 0$ and $\tilde{J}_h \to 0$ should give identical expressions after an exchange of the subscripts l and h, and this is not the case here. However, the results differ only by numerical coefficients that are $O(1)$, and this may count as a useful approximation in many cases.

The result eq. 35 shows that Ohmic heating, like collisionless heating, is enhanced by the combination of two frequencies. The physical mechanism of the enhancement is similar—when the lower frequency is applied, the spatial structure of the sheath region is modified, and in particular the ion density near the boundary is greatly reduced. When the sheath is collapsed, and these regions are populated by electrons, the higher frequency current is conducted through a much more tenuous plasma than would be the case if the lower frequency was absent. The Ohmic heating effect is thereby dramatically enhanced.

4. Ohmic and collisionless heating

Typical dual frequency discharges will be excited by some combination of collisionless and Ohmic heating. The superposition of these two heating mechanisms can produce a rather complex spatio-temporal pattern. Some indication of this is shown in fig. 9, which shows the total electron heating as a function time, integrated over the quasi-neutral part of the sheath region. The data shown in this figure include not only the collisionless heating and the Ohmic heating discussed above, but also the terms associated with the oscillation of the electron drift velocity and temperature within the sheath region. These last two terms do not contribute any net heating, but they are an appreciable part of the instantanous power.

We have seen that both collisionless and Ohmic heating are enhanced when currents at two disparate frequencies are superimposed, and that the mechanism of this enhancement is the control over the sheath structure exerted by the lower frequency in combination with the higher current density associated with the higher frequency. Inspection and comparison of eqs. 20 and 35 suggests that the enhancement effect on the Ohmic heating will prove stronger, at least when H_l is large. This indeed the case. Fig. 10 shows the time-averaged collisionless and Ohmic heating components, with the total heating, as a function of the low-frequency current density, with all other parameters held constant. It is clear that the application of the low-frequency current can produce a transition from a situation that is dominated by collisionless heating to one dominated by Ohmic heating. Of course, whether this occurs or not also depends

on the neutral gas pressure, and in fig. 11 we show the ratio of collisionless to Ohmic heating as a function of low-frequency current density for three disparate gas pressures, covering probably the entire range of practical interest. These data show that it is rather unlikely that a dual frequency discharge used for plasma processing will be dominantly heated by collisionless processes. For example, a typical operating pressure for a dual frequency etching discharge is ~ 50 mTorr, under which condition probably much more than half of the net heating power is Ohmic.

5. Concluding Remarks

In this paper we have developed approximate expressions for collisionless and Ohmic heating of electrons in dual-frequency discharges. These expressions show that both kinds of heating are much affected by the low-frequency current density, because the large voltage associated with that current is the dominant influence on the spatial structure of the sheath region. Although both heating mechanisms are enhanced by the low-frequency current, the effect on Ohmic heating is stronger, with the implication that the dominant heating mechanism can be changed. Indeed, under typical experimental conditions, a discharge that would be dominated by collisionless heating in the absence of a low-frequency component in the current can become Ohmically dominated when the low-frequency current is applied.

We have neglected a number of issues that may need to be considered in future work. For example, we have assumed that electromagnetic [23] and resonant phenomena [24] may be ignored. We believe this to be reasonable under most experimental conditions today. However, there is a tendency towards increasing the higher frequency in industrial practice, which if continued could vitiate these assumptions. At the moment, nothing is known of the heating mechanisms that might be dominant at very high frequencies. We have also taken rather simple view of the effect of friction on the sheath dynamics. For example, it is known that under some conditions, the sheath electric field may reverse [25], with sometimes dramatic effects on electron heating. Such effects could occur in dual-frequency discharges.

[1] H. C. Kim, J. K. Lee, and J. W. Shon. Analytic model for a dual frequency capacitive discharge. *Phys. Plasmas*, 10(11):4545–4551, November 2003.

[2] P. C. Boyle, A. R. Ellingboe, and M. M. Turner. Independent control of ion current and ion impact energy onto electrodes in dual frequency plasma devices. *J. Phys. D: Appl. Phys.*, 37:697–701, 2004.

[3] F. A. Haas. A simple model of an asymmetric capacitive plasma with dual frequency. *J. Phys. D: Appl. Phys.*, pages 3117–3120, 2004.

[4] J. K. Lee, N.Y. Babaeva, H. C. Kim, O. V. Manuilenko, and J. W. Shon. Simulation of capacitively coupled single- and dual-frequency rf discharges. *IEEE Trans. Plasma Sci.*, 32(1):47 – 53, 2004.

[5] H. C. Kim and J. K. Lee. Mode transition induced by low-frequency current in dual- frequency capacitive discharges. *Phys. Rev. Lett.*, 93(8):085003, 2004.

[6] H. C. Kim and J. K. Lee. Dual frequency capacitive discharges: Effect of low-frequency current on electron distribution function. *Phys. Plasmas*, 12:053501, 2005.

[7] G. Gozadinos, D. Vender, M. M. Turner, and M. A. Lieberman. Collisionless electron heating by capacitive radio-frequency sheaths. *Plasma Sources Sci. Technol.*, 10:1–8, 2001.

[8] Igor D. Kaganovich. Anomalous capacitive sheath with deep radio frequency electric field penetration. *Phys. Rev. Lett.*, 89:265006, 2002.

[9] M. M. Turner and P. Chabert. Collisionless heating in capacitive discharges enhanced by dual frequency excitation. *Phys. Rev. Lett.*, 96(20):205001, May 2006.

[10] E. Kawamura, M. A. Lieberman, and A. J. Lichtenberg. Stochastic heating in single and dual frequency capacitive discharges. *Phys. Plasmas*, 13(5):053506, May 2006.

[11] Igor D. Kaganovich, Oleg V. Polmarov, and Constantine E. Theodosiou. Revisiting the anomalous RF field penetration into a warm plasma. *IEEE Trans. Plasma Sci.*, 34(3):696–717, June 2006.

[12] Michael A. Lieberman and Allan J. Lichtenberg. *Principles of Plasma Discharges and Materials Processing*. Wiley, New York, 1994.

[13] J. Robiche, P. C. Boyle, M. M. Turner, and A. R. Ellingboe. Analytical model of a dual frequency capacitive sheath. *J. Phys. D: Appl. Phys.*, 36:1810–1816, 2003.

[14] R. N. Franklin. The dual frequency radio-frequency sheath revisited. *J. Phys. D: Appl. Phys.*, 36:2660–2661, 2003.

[15] P. C. Boyle, J. Robiche, and M. M. Turner. Modelling of the dual frequency capacitive sheath in the intermediate pressure range. *J. Phys. D: Appl. Phys.*, 37:1451–1458, 2004.

[16] Kazuki Denpoh, Go Wakayama, and Kenichi Nanbu. Sheath model for dual-frequency capacitively coupled plasmas. *Jpn. J. Appl. Phys.*, 43(8A):5533–5539, 2004.

[17] M. A. Lieberman. Analytical solution for capacitive rf sheath. *IEEE Trans. Plasma Sci.*, 16(6):638–644, December 1988.

[18] C. K. Birdsall and A. B. Langdon. *Plasma Physics via Computer Simulation*. McGraw-Hill, New York, 1985.

[19] G. Gozadinos, D. Vender, and M. M. Turner. Boundary conditions and particle loading for the modeling of a semi-infinite plasma. *J. Comp. Phys.*, 172(1):348–355, September 2001.

[20] M. Surendra and D. B. Graves. Electron acoustic waves in capacitively coupled, low-pressure rf glow discharges. *Phys. Rev. Lett.*, 66(11):1469–1472, March 1991.

[21] M. M. Turner. Pressure heating of electrons in capacitively-coupled rf discharges. *Phys. Rev. Lett.*, 75(7):1312–1315, August 1995.

[22] M. A. Lieberman. Dynamics of a collisional, capacitive RF sheath. *IEEE Trans. Plasma Sci.*, 17(6):338, December 1989.

[23] P. Chabert, J. L. Raimbault, P. Levif, J. M. Rax, and M. A. Lieberman. Inductive heating and E to H transitions in capacitive discharges. *Phys. Rev. Lett.*, 95(20):205001, November 2005.

[24] T Mussenbrock and R-P. Brinkmann. Nonlinear electron resonance heating in capacitive radio frequency discharges. *Appl. Phys. Lett.*, 88(15):151503, April 2006.

[25] M. M. Turner and M. B. Hopkins. Anomalous sheath heating in a low-pressure rf discharge in nitrogen. *Phys. Rev. Lett.*, 69(24):3511–3514, December 1992.

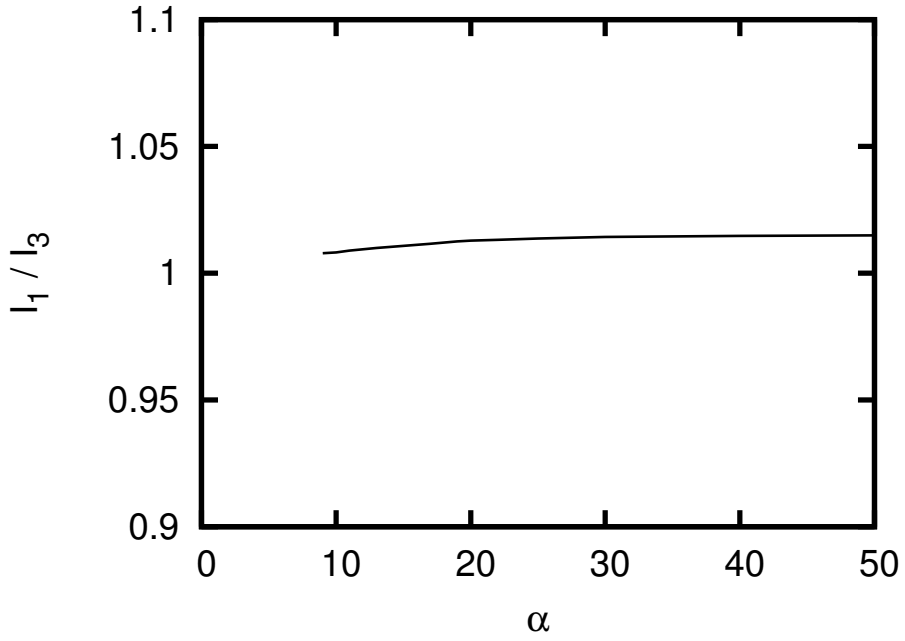

Figure 1. Comparison of the value of the integral F_1 determined by a quadrature with the approximation to A_1 given by eq. 19. The parameters held fixed are $H_l = 11$ and $\beta = 3.6$.

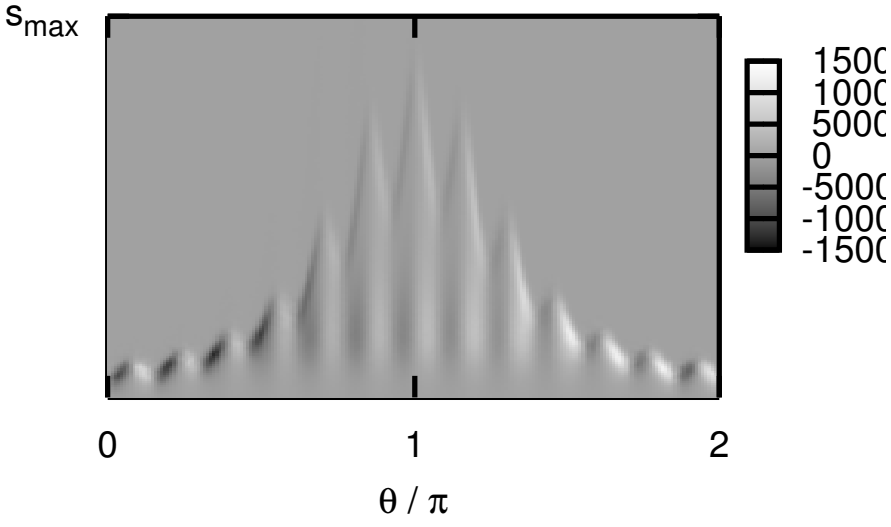

Figure 2. Collisionless heating power as a function of space and time, calculated by the particle simulation, with $\tilde{J}_l = 10$ A m^{-2}, $\omega_l = 2\pi \times 2$ MHz, $\tilde{J}_h = 20$ A m^{-2} and $\omega_l = 2\pi \times 26$ MHz, and the plasma parameters discussed in the text. The ion sheath edge is at $x = 0$ and the electrode is at $x = s_{\max}$.

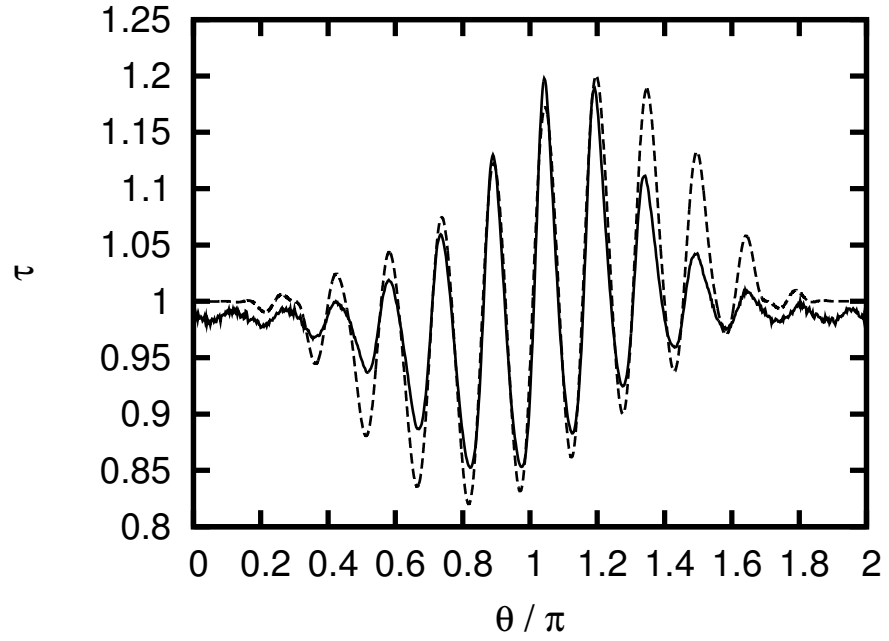

Figure 3. Temperature of electrons in the sheath computed from the analytic theory of the text (solid line) and from the particle-in-cell simulation (dashed line), for the conditions noted in fig. 2.

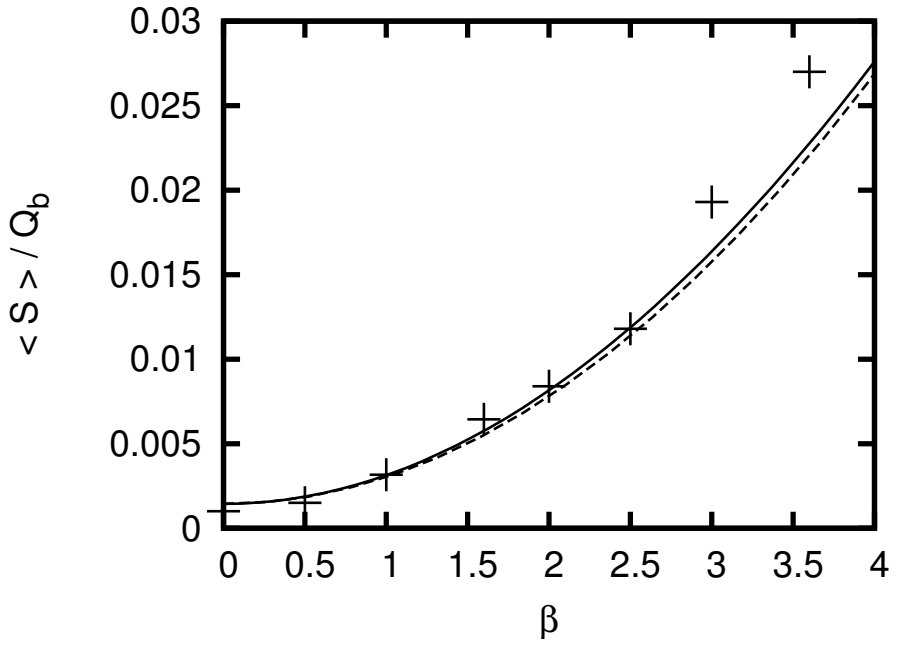

Figure 4. Normalized collisionless heating power as a function of $\beta \equiv \tilde{J}_h/\tilde{J}_l$, with $\tilde{J}_h$ as the parameter varied (so that H_l is constant) and with $\alpha = \omega_h/\omega_l = 13$.

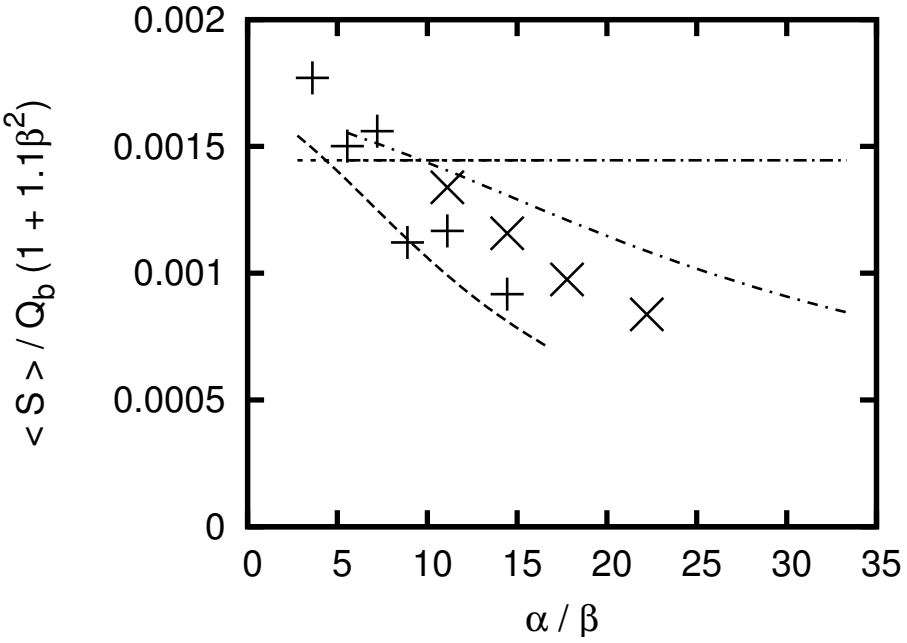

Figure 5. Normalized collisionless heating power as a function of $\alpha/\beta \equiv \omega_h \tilde{J}_l / \omega_l \tilde{J}_h$, with ω_h and $\tilde{J}_h$ as the parameters varied (so that H_l is constant). Simulation data are shown by points for two values of β, corresponding to $\tilde{J}_h = 18$ A m^{-2} and 36 A m^{-2}. ω_h is in the range $2\pi\times$ 26 MHz to $2\pi\times$ 104 MHz. The flat lines is the predictions of eq. 20, the sloping lines are derived from numerical solutions of eq. 6.

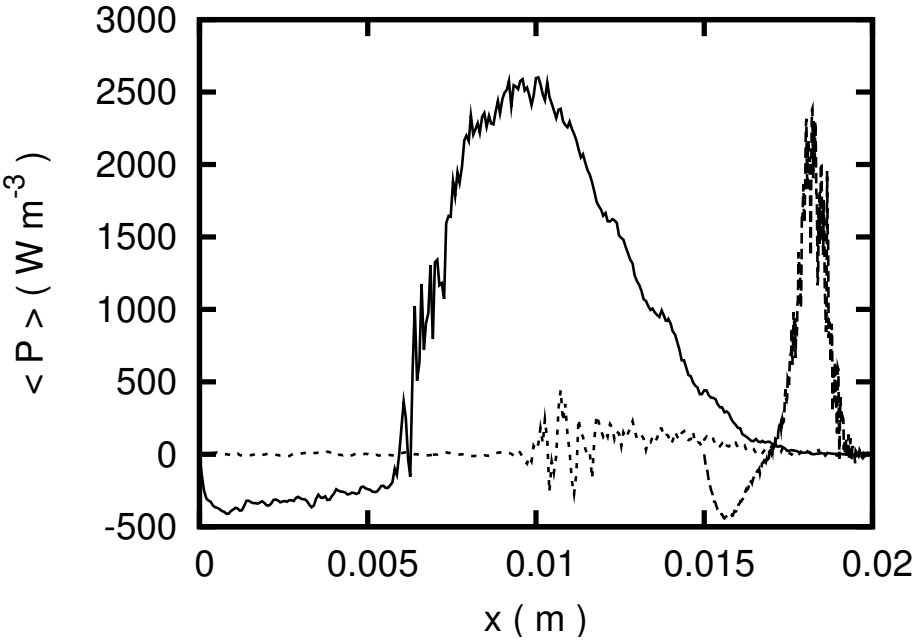

Figure 6. Time averaged electron heating power resolved in space for three cases corresponding to the two frequencies acting separately and both acting together. Note that the ion sheath edge in each case is approximately located at the transition to negative power absorption, and that the sheath width is appreciably influenced by the application of the high frequency [13], relative to the low frequency acting alone. The parameter values used are $\tilde{J}_l = 10$ A m^{-2}, $\omega_l = 2\pi \times 2$ MHz, $\tilde{J}_h = 36$ A m^{-2} and $\omega_l = 2\pi \times 26$ MHz.

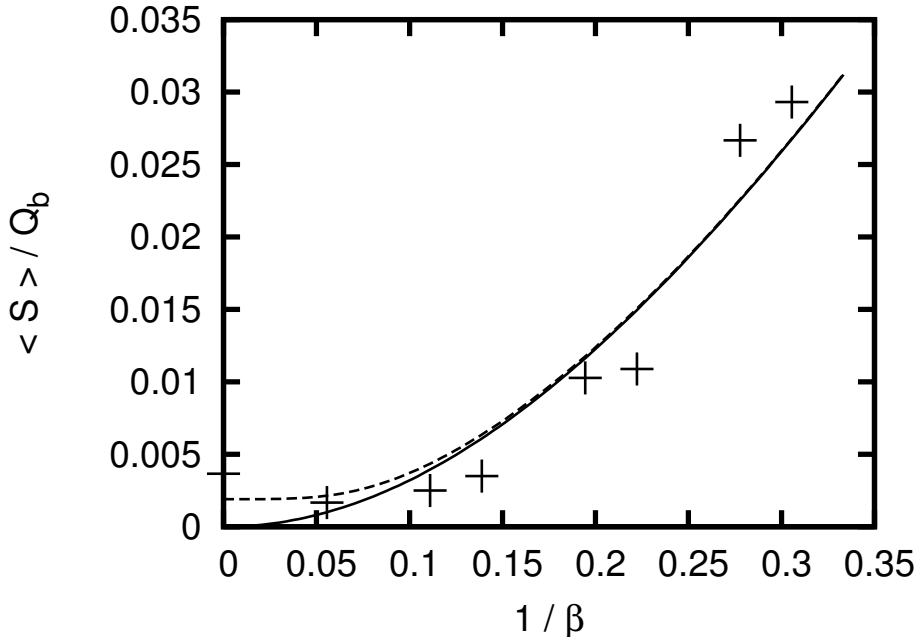

Figure 7. Time averaged electron heating power as a function of $1/\beta \equiv J_l/J_h$, where the parameter varied is the low frequency current density J_l. Other parameters held constant are the high frequency current density $J_h = 36$ A m^{-2}, and the two frequencies $\omega_l = 2\pi \times 2$ MHz and $\omega_h = 2\pi \times 26$ MHz.

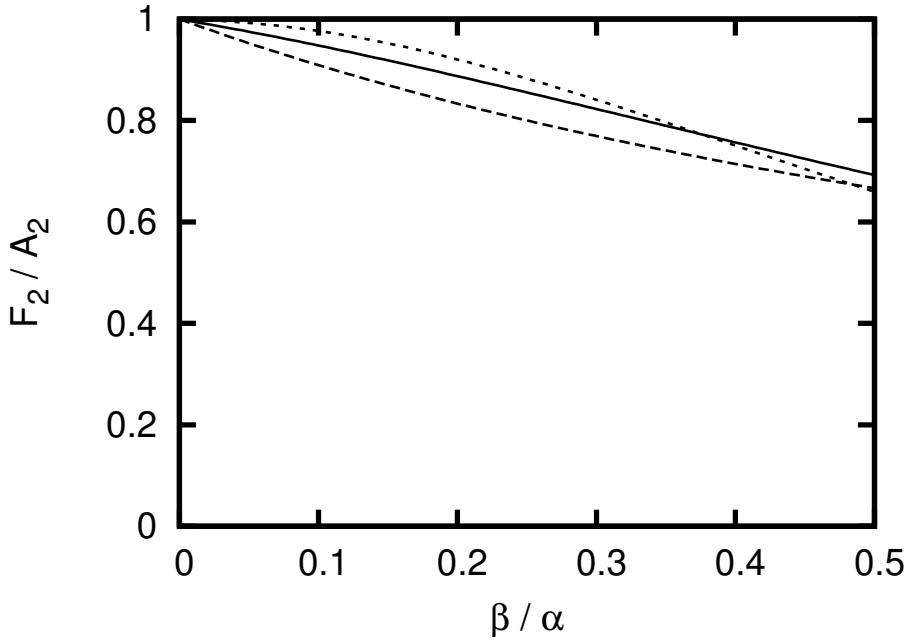

Figure 8. The approximation given by eqn. 35 compared with numerical evalution of the integral in eqn. 34, for various parameters. Solid line, $H_l = 1$, $\alpha = 100$; Long dashed line, $H_l = 0$, $\alpha = 10$; Short dashed line, $H_l = 11$, $\alpha = 20$

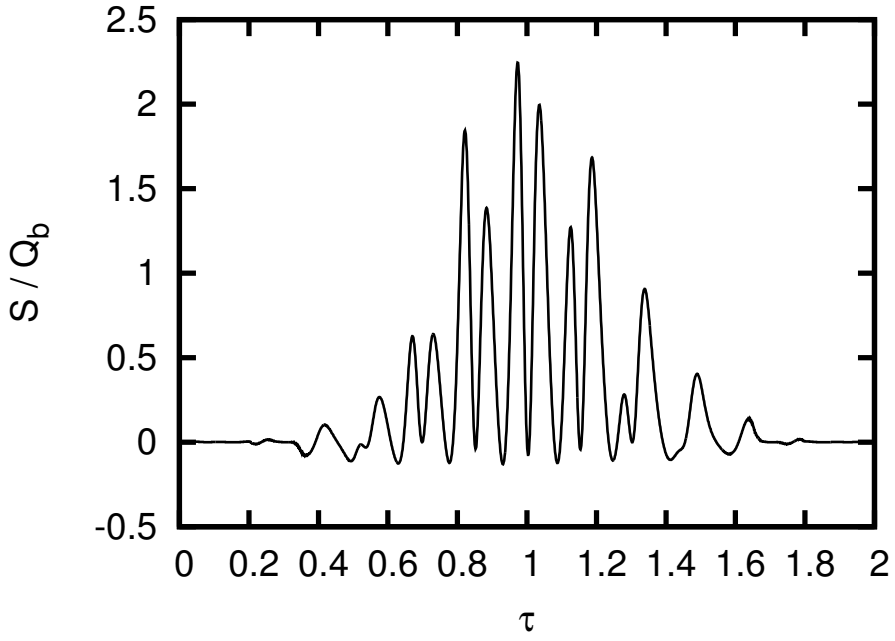

Figure 9. The spatially integrated electron heating power in the sheath, including the collisionless, inertial, and Ohmic components, with $\omega_l/2\pi = 2$ MHz, $\omega_h/2\pi = 26$ MHz, $\tilde{J}_h = 36$ A m^{-2}, $\tilde{J}_l = 2$ A m^{-2},$n_0 = 5 \times 10^{15}$ m^{-3}, $T_b = 30000$ K, and $\nu_e/\omega_l = 30$.

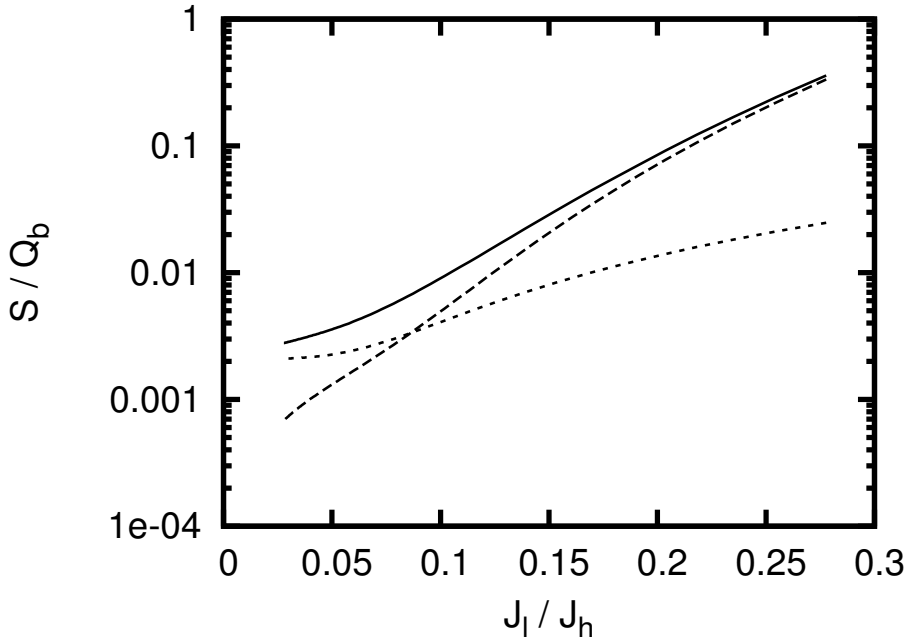

Figure 10. The collisionless, Ohmic and total heating powers, shown as a function of the low frequency current density. Solid line—total; long dashed line—Ohmic; short dashed line—collisionless. Conditions as for fig. 9, apart from $\tilde{J}_l$

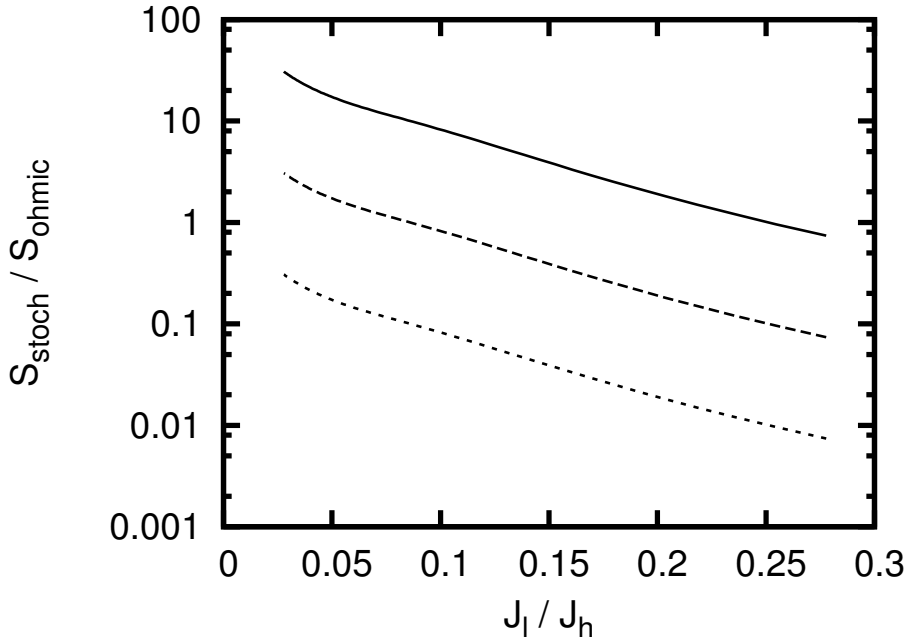

Figure 11. The ratio of the collisionless and Ohmic heating powers for various electron collision frequencies, corresponding approximately to conditions in argon at pressures of 10 (solid line), 100 (long dashed line) and 1000 mTorr (short dashed line) corresponding to $\nu_e/\omega_l = 3, 30, 300$. Conditions as for fig. 9, apart from $\tilde{J}_l$ and ν_e.